GEOLOGY

Melting of sediments in the deep mantle produces saline fluid inclusions in diamonds

Michael W. Förster[1]*, Stephen F. Foley[1], Horst R. Marschall[2], Olivier Alard[1,3], Stephan Buhre[4]

Diamonds growing in the Earth's mantle often trap inclusions of fluids that are highly saline in composition. These fluids are thought to emerge from deep in subduction zones and may also be involved in the generation of some of the kimberlite magmas. However, the source of these fluids and the mechanism of their transport into the mantle lithosphere are unresolved. Here, we present experimental results showing that alkali chlorides are stable solid phases in the mantle lithosphere below 110 km. These alkali chlorides are formed by the reaction of subducted marine sediments with peridotite and show identical K/Na ratios to fluid inclusions in diamond. At temperatures >1100°C and low pressures, the chlorides are unstable; here, potassium is accommodated in mica and melt. The reaction of subducted sediments with peridotite explains the occurrence of Mg carbonates and the highly saline fluids found in diamonds and in chlorine-enriched kimberlite magmas.

INTRODUCTION

The lithospheric mantle beneath the cratons (*1*) contains a complex record of geochemical depletion by ancient melting events that are overprinted by later refertilization by infiltrating liquids (*2*, *3*). Fast-growing fibrous diamonds, and less often, gem-quality diamonds (*4*), trap and preserve fluids that are present during their formation, providing insights into the chemical environment of diamond formation (*5*, *6*). The encapsulated fluids may be highly saline, with K/Na ratios (by mass) of 1:1 to 9:1, siliceous, or low- or high-Mg carbonatitic in composition (*2*, *7*–*9*). However, the source of these exotic fluids within the lithospheric mantle has remained ambiguous (*4*, *7*, *8*). Weiss *et al.* (*2*) argue that the saline component in diamond micro-inclusions originates from subducted seawater in altered oceanic crust, but the mechanism of fluid transport and the fractionation of K from Na remain enigmatic.

Diamonds (*10*) are transported to the surface by kimberlites, which are rapidly emplaced magmas with exotic H_2O- and CO_2-rich compositions and whose origin is still a matter of debate (*11*–*14*). Melting experiments on peridotite with H_2O and CO_2 can explain the carbonate component in kimberlites but cannot reproduce the high K/Na unless the starting composition is preenriched in K_2O (*15*). The most recent models explain kimberlites as hot (>1400°C) melts of peridotite (*16*, *17*), whereas other authors argue for cooler primary melts from a carbonated peridotite and Na carbonatite chloride compositions with low emplacement temperatures (<800°C) (*18*). The models that advocate primary kimberlite magmas similar to carbonatites suggest that kimberlitic melts are similar to the high-Mg saline, carbonatitic micro-inclusions in diamonds (*18*, *19*). However, the micro-inclusions show higher contents of alkalis, even when compared to the most alkaline kimberlite, Udachnaya-East (*18*), and highly saline fluids may play only a restricted role in shaping the source of many kimberlites. The Udachnaya-East kimberlite is also globally prominent because of its abundant chloride phases and may have been formed from an unusual chloride-rich source (*18*). In addition to fluid inclusions, diamonds contain mineral inclusions, with compositions indicative of the rock type in which they formed (*7*, *9*). These include olivine, chromite, orthopyroxene, clinopyroxene, and garnet sourced from mantle peridotites, as well as omphacite, a characteristic phase of eclogite, which results from basalt or gabbro being metamorphosed at high pressures (*20*).

In this study, we conducted two types of experiments: a melting experiment on marine sediments and reaction experiments using a two-layer arrangement in which marine sediment and a geochemically depleted peridotite (dunite) were loaded as distinct blocks in single experimental capsules. Experiments were conducted at 3 to 6 GPa and 800° to 1100°C, corresponding to a depth of 100 to 200 km in the mantle (table S1). Generally, subducted crustal rocks have solidus temperatures as low as 675°C, which depend on pressure and particularly on volatile contents (*21*–*23*). The experiments were all conducted above the solidus of the marine sedimentary rock, while the experiment at 3 GPa/800°C is close to the solidus, as indicated by the small melt fraction of ~10% (fig. S1). In subduction zones, slab-surface temperatures vary strongly with age, speed, and angle of subduction (*24*). Hence, the deep subduction of sediments to cratonic mantle depths is most probable in the case of an old cold slab. Because substantial element transport from subducted sediments to the mantle wedge only occurs above the solidus (*22*), sediment subduction to the deep mantle is feasible in a cold slab. The experiments presented here trace this scenario, simulating the reaction of sediments that melt only after rapid subduction to a depth of >100 km.

RESULTS

Here, we present the results of an experimental study that simulates the reaction of subducted marine sediments with mantle peridotite at pressures corresponding to the mid-cratonic to lower cratonic lithosphere. The results shed light on the origin of exotic diamond fluid compositions. All reaction experiments resulted in a reaction zone situated between the two rock types, whereby the former sediment layer that recrystallized to garnet and clinopyroxene (Fig. 1, A and B); these reaction zones contain Na-K chlorides in experiments at pressures

[1]ARC Centre of Excellence of Core to Crust Fluid Systems and Department of Earth and Planetary Sciences, Macquarie University, Sydney, NSW 2109, Australia. [2]Institut für Geowissenschaften, Goethe Universität, 60438 Frankfurt am Main, Germany. [3]Géosciences Montpellier, UMR 5243, CNRS & Université Montpellier, 34095 Montpellier, France. [4]Institut für Geowissenschaften, Johannes Gutenberg Universität, 55099 Mainz, Germany.
*Corresponding author. Email: michael.forster@mq.edu.au

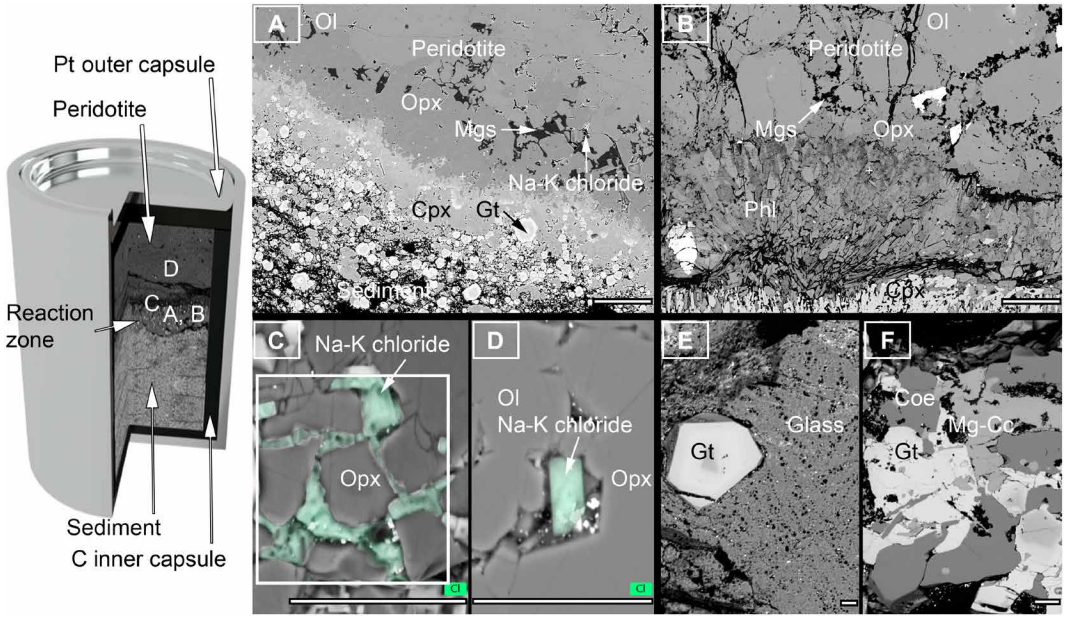

Fig. 1. Backscattered electron images of experimental charges. Locations of images (**A**) to (**D**) from sediment-peridotite reaction experiments are schematically shown in capsule on the left. (A, C, and D) Reaction experiments at 5 GPa/1000°C with superimposed energy-dispersive x-ray maps of chlorine [green in (C) and (D)]. The sediment half of two-layer experiments recrystallized to garnet and clinopyroxene (Cpx), whereas orthopyroxene (Opx), magnesite (Mgs), and Na-K chlorides formed at the leading edge of the reaction zone against the peridotite. (B) Peridotite layer in the reaction experiment at 3 GPa/900°C contained phlogopite (Phl) behind the magnesite + orthopyroxene zone, and Na-K chlorides were absent. (**E** and **F**) Sediment melting experiment (no peridotite included) at 4 GPa/1000°C showing silicate melt (E) in equilibrium with garnet (Gt), coesite (Coe), and Mg calcite (Mg-Cc) shown in (F). Scale bars, 100 μm (A and B) and 20 μm (C to F).

at and above 4 GPa (Fig. 1, A, C, and D, and figs. S1 to S4). Most of the analyzed chlorides contain 5 to 15 weight % (wt %) Na and 30 to 45 wt % K, with K/Na ratios between 2:1 and 9:1 (by mass; Fig. 2). In contrast, all reaction experiments at 3 GPa and the higher temperature experiment at 4 GPa/1100°C, as well as the sediment melting experiment at 4 GPa/1000°C, are devoid of chlorides. In these experiments, potassium and sodium are contained in phengite, Mg-rich mica (phlogopite), and melt (Fig. 1, B, E, and F). The melts are silica rich (>55 wt % SiO_2), containing 0.2 to 0.4 wt % chlorine and exhibiting K/Na ratios of 3:1 to 7:1. However, melt and mica do not account for all chlorine in the starting sediment composition, just as the low abundance of Na-K chlorides of ~0.5% does not contain all Na and K in mica- and melt-free experiments. Mass balance calculations show that the experiments contain a Cl, F–enriched fluid phase depleted in K at <4 GPa and >1000°C, whereas fluids in equilibrium with Na-K chlorides are Cl, F–depleted and enriched in Na and K (Supplementary Materials). Light element analysis of the sedimentary starting material shows C, H, and N mass fractions of 8.2 ± 0.1, 1.8 ± 0.2, and 0.35 ± 0.01 wt %, respectively, which are sourced from carbonate, clay minerals, and organic material. The loss on ignition of 15.3 wt % gives an oxygen mass fraction of ~6.9 wt % by subtracting carbon, hydrogen, and nitrogen and addition of oxygen from SO_3 and Fe_2O_3 reduction (table S2). The breakdown of carbonate, clay, and organic material would thus produce a mixed $H_2O \pm H_2 \pm CO_2 \pm CO \pm CH_4$ fluid, the speciation of which depends strongly on pressure, temperature, and oxygen fugacity. Given carbon saturation, the decomposition of the sediment follows the reaction: $CH_4 + H_2O = 3\ H_2 + CO$ (*25*). Because equilibrium constants are undetermined for the experimental pressure range, the measured mass fractions of 8.2 wt % C, 1.8 wt % H, and 6.9 wt % O will fall within a range for each species at the beginning of the reaction: 4.0 to

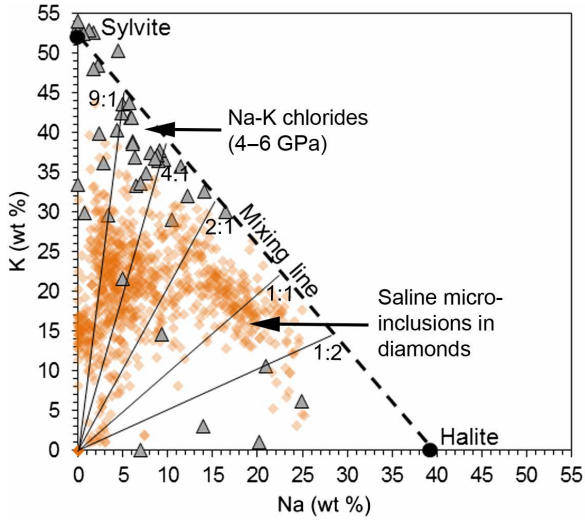

Fig. 2. K/Na ratios of experimental chlorides and saline micro-inclusions in diamonds. Most saline micro-inclusions (orange diamonds) (*2*, *7*, *30*) have a K/Na ratio between 1:1 and 9:1, similar to the ratios found in the experimental Na-K chlorides of this study (gray diamonds). Full analyses of chlorides are given in tables S9 to S12.

5.3 wt % CH_4, 9.7 to 12.0 wt % CO, 0 to 1.5 wt % H_2O, 0 to 0.5 wt % H_2. Because of the graphite inner capsule, which provides excess C, the C species change during the experiments. The graphite inner capsule also buffers the oxygen fugacity at C-CO, and the equilibrium $2\ CO = C + CO_2$ leads to CO_2 formation at all relevant thermobaric conditions (*26*). At T < 1000°C, CO_2 reacts with olivine to form magnesite and orthopyroxene: $Mg_2SiO_4 + CO_2 = MgCO_3 + MgSiO_3$,

which is in accordance with the presence of <7 wt % magnesite in the reaction zones (fig. S1).

Besides magnesite, the reaction zone in all experiments at <1100°C is also enriched in clinopyroxene (Fig. 1, A and B). These clinopyroxenes exhibit a gradual change in composition from high Na_2O (~5 wt %) and Al_2O_3 (~10 wt %) in the former sedimentary rock to low Na_2O (~0.6 wt %) and Al_2O_3 (~3 wt %) in the peridotite (fig. S5A). Micas also fall into two groups based on their Al and Ti contents: Those from experiments at 1000° to 1100°C contain 13 to 16 wt % Al_2O_3 and 1 to 2 wt % TiO_2, whereas in experiments at lower temperatures they contain lower Al_2O_3 (8 to 13 wt %) and TiO_2 (0.5 to 1 wt %) (fig. S5B).

DISCUSSION

If the fluids found as micro-inclusions in diamond ultimately originated from seawater in subducting sediments, then a process that very efficiently fractionates Na^+ from K^+ is required to explain their high K/Na ratios of 1:1 to 9:1. Weiss *et al.* (*2*) postulated that Na^+ is consumed during low-temperature alteration of seafloor basalts and that K/Na is increased further by the formation of Cl^--rich phengite. Our experimental results show that the fractionation of Na^+ from K^+ can also occur at high pressures in liquids that originate from the reaction between subducted marine sediments and peridotite; this is in accordance with previous results that show a gradual increase of K/Na in fluids and melts with pressure and temperature (*22*). The Na-K chlorides formed only in reaction experiments conducted at 4 to 6 GPa and <1100°C, giving way to Cl-bearing mica and silicate melt at lower pressure and higher temperature (Fig. 3). The restriction of chlorides to the reaction experiments (they do not occur in the melting experiment on the sedimentary rocks) shows that these phases are only stable in an ultramafic, high-pressure environment (fig. S1). The euhedral appearance of cubic chloride crystals is indicative of equilibrium growth from highly saline fluids rather than forming as a quench phase (Fig. 1D), which would result in a mat of interlocking crystals at random angles, as seen in many high-pressure experiments (*14*). While the capsule setup in this study does not allow for direct measurement of the fluid composition, the mass balance calculation estimates K/Na of the fluid to be 4.5 ± 3.6 (Supplementary Materials), which is within the average K/Na of 7.3 ± 5.9 of the Na-K chlorides. The fluid has to be enriched in K because Na is sequestered in abundant, coexisting Na-rich clinopyroxene and K is absent in any other phase than the Na-K chlorides in the reaction experiments at 4 to 6 GPa (fig. S1). Because the Na-K chlorides only account for ~20% of the total mass fraction of K in the experiments, a K/Na-rich fluid has to be present during the crystallization of the chlorides. It also has to be emphasized that all chloride-bearing experiments are devoid of any hydrous phase. It is thus likely that the process of chloride formation is restricted to a reducing environment and a shift in fluid species, which consumes H_2O following the reactions: $CH_4 + H_2O = 3\ H_2 + CO$ and $2\ CO = C + CO_2$. The reaction also produces C, because the removal of CO_2 shifts the equilibrium on the product side of the second equation. The coexistence of elemental C with CO_2 and magnesite has been previously observed in diamond inclusions (*27*). Thus, the sequestration of CO_2 in magnesite is related to the consumption of $CH_4 + H_2O$ until H_2O is exhausted. Hence, Na-K chlorides form by precipitation from an oversaturated solution: $Na/K^+(aq) + Cl^-(aq) = (Na,K)Cl$.

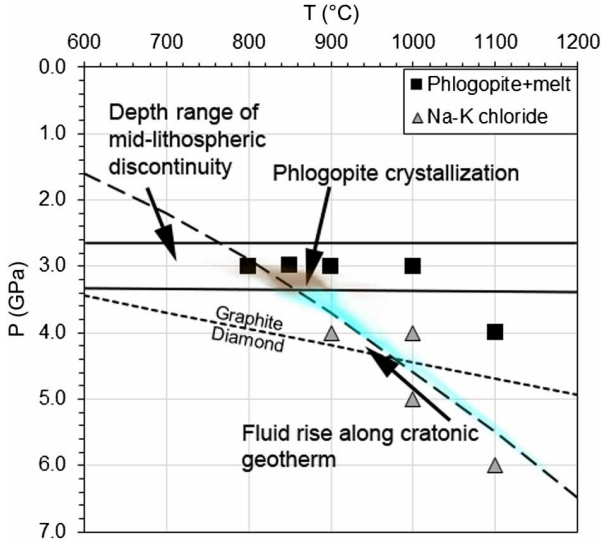

Fig. 3. Pressure-temperature stability of Na-K chlorides. Na-K chlorides are restricted to reaction experiments at 4 to 6 GPa, while at 3 and 4 GPa/1100°C, K is sequestered in phlogopite. When mobile, highly saline fluids (blue) rise to lower pressures along the cratonic geotherm, they stall and react to form phlogopite-bearing metasomes (brown). The depth of phlogopite crystallization coincides with the mid-lithospheric discontinuity (*32*).

The crystallization of Na-K chlorides is induced by the reducing conditions in the inner graphite capsule, and any experimental buffer material at fO_2 (oxygen fugacity) equal to or below CCO will lead to chloride formation. In contrast, at any fO_2 above CCO, H_2O will not be exhausted and Na, K, and Cl stay in solution to form the known highly saline fluids. Given the low fO_2 that is needed for chloride precipitation, magnesite and H_2 may be expected to react: $MgCO_3 + H_2 = Mg(OH)_2 + CO$. However, the process of carbonate reduction is known to be kinetically slow, especially at high pressure (*28*, *29*). Because the dehydration of the fluid is only observed in reaction experiments at >3 GPa, the sequence leading to chloride precipitation has to be as follows: (i) melting of the sediment and reaction with dunite; (ii) total consumption of the melt phase by anhydrous phases (garnet and pyroxene) as evident from mass balance calculations (figs. S1 and S2), which drives all H_2O into a fluid phase; and (iii) dehydration of the fluid by reaction of H_2O to H_2 and precipitation of chloride from a fluid saturated in K, Na, and Cl. If fO_2 is above CCO, then Na-K chlorides will not precipitate but instead will be dissolved in highly saline hydrous fluids. The absence of hydrous crystalline phases such as mica in all chloride-bearing experiments is thought to be a direct result of the depletion of the fluid in H_2O, although depletion of Al by the increasing modal abundance of garnet at >3 GPa cannot be discounted.

The K/Na ratios of the chlorides (1:2 to 9:1) largely overlap with those of saline fluids included in diamonds (1:1 to 9:1; Fig. 2). The Cl/(Na + K) of Na-K chlorides give 1.03 ± 0.44, which is comparable to the values of 1.05 ± 0.36 measured for saline fluids. However, the fluid micro-inclusions in diamond show lower total mass fractions of Na^+ and K+ (*2*, *7*, *30*), and thus may represent diluted equivalents of the chlorides (i.e., they are closer to the origin in Fig. 2). Silicate melts in experiments at 3 GPa attain K/Na ratios of 3:1 to 7:1, indicating that the process of Na separation and K enrichment in the melt is equal to the processes that lead to high K/Na chlorides. All reaction experiments

contain clinopyroxene, which shows an increase in Na and Al across the reaction zone from the peridotite toward the sediment (fig. S5A). We argue that the enrichment of K/Na in melts and chlorides is caused by the contemporaneous crystallization of Na-Al–rich clinopyroxene in the former sedimentary rock, transforming it to a Na-enriched residuum with low K/Na ratios. Similar clinopyroxenes rich in Na and Al are found in natural mantle xenoliths that occur in kimberlites such as Udachnaya-East (*31*). These sodic, aluminous clinopyroxenes are of metasomatic origin and are geochemically distinct from peridotite clinopyroxenes (fig. S5A). In the 3-GPa experiments, clinopyroxene coexists with mica, which is also comparable to mica found in the metasomatic Udachnaya-East xenoliths (fig. S5B) (*31*).

The formation of Mg carbonates, and of chlorides with high K/Na, demonstrates that the reaction between sediment and peridotite may cause a type of mantle metasomatism that is vital for the formation of some diamonds. The compositions of saline micro-inclusions in diamonds are distributed between four end-members: a Na-K chloride–enriched composition, low- and high-Mg carbonatitic, and silicic compositions (Fig. 4). Weiss *et al.* (*2*) interpret this suite to represent mixing of highly saline fluids from the subducting slab with carbonated peridotite and eclogite. From our experimental observations, we argue that the carbonate is also derived from the sediment and forms by the reaction of CO_2-bearing saline fluids with mantle peridotite. This process consumes CO_2, which is incorporated into Mg carbonate (magnesite) that grows at the expense of olivine at the reaction front (Fig. 1, A and B). Because magnesite is the only observed carbonate phase within the peridotite, the metasomatically overprinted mantle would preferentially produce high-Mg carbonatitic melt if remelted at a later stage. In a natural setting, diamonds would grow during the reaction that produces the magnesite and enclose fluids from various stages of this interaction. If "most diamonds were created equal" (*4*), then it would follow that the reaction between sedimentary rocks and peridotite during subduction is a main mechanism for the formation of lithospheric diamonds and mantle carbonates.

The high mobility of saline fluids provides an effective mechanism to metasomatize the cratonic lithosphere. Na-K chlorides and carbonates are widely distributed in the reaction zone and the peridotite in the experiments, whereas the growth of mica in halide-free experiments is restricted to the reaction zone (Fig. 1B). This demonstrates that Na-K chlorides and carbonates crystallized from highly mobile fluids. Our experimental delineation of alkali chloride stability restricts this to depths greater than approximately 120 km, spreading to shallower depths where temperatures are lowest. Fluids that move far from their source are strongly depleted in all major elements except for the highly fluid-soluble alkalis and magnesium, because only magnesite and chlorides are observed within the peridotite layer (Fig. 1, A, C, and D). This means that radiogenic isotope and geochemical signatures of the sediment probably remain sequestered in clinopyroxene in the reaction zone. Hence, if Sr and Eu are mostly retained in clinopyroxene, then the fluid that progresses into the peridotite should have gradually flatter positive Sr and Eu anomalies as well as evolving to lower $^{87}Sr/^{86}Sr$ ratios (*2*).

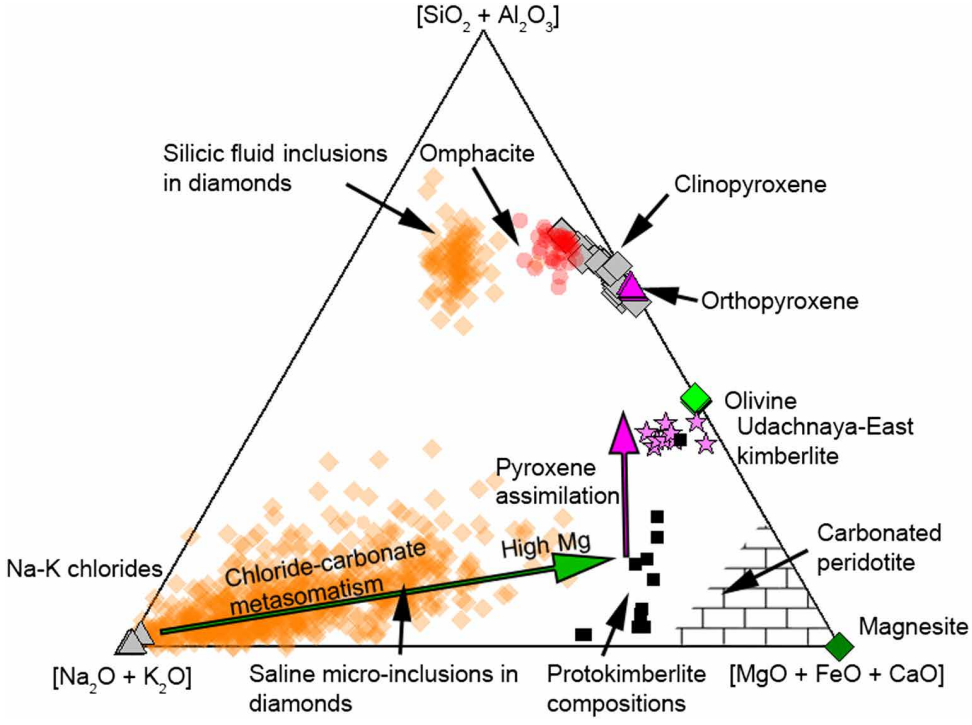

Fig. 4. Ternary diagram of experimental phase compositions compared to diamond inclusions. Composition of saline and silicic diamond micro-inclusions (orange diamonds) (*2*, *7*, *9*, *30*) and omphacite mineral inclusions in diamonds (red circles) (*2*) compared to clinopyroxenes (light gray diamonds), orthopyroxenes (pink triangles), olivines (green diamonds), magnesite (olive diamonds), and Na-K chlorides (gray triangles) from this study. The "carbonated peridotite" field represents various mixtures of Mg carbonate (magnesite) and silicates. Saline micro-inclusions are mixtures between the Na-K chloride and carbonated peridotite (green arrow). The source for protokimberlitic melts of Udachnaya-East (black squares) (*40*) is enriched in Na and K relative to carbonated peridotite and trends toward bulk kimberlite composition (pink stars) (*44*) by assimilating pyroxenes, as indicated by the pink arrow.

The change of style of metasomatic overprinting in the depleted peridotite from highly saline fluids and chlorides at ≥4 GPa to melt infiltration and mica formation below 4 GPa has further consequences for the cratonic mantle: Fluids that rise to mantle levels shallower than the stability of Na-K chlorides will stall and crystallize mica, as evident from reaction experiments at 3 GPa (Fig. 3). The depth at which these highly saline fluids stall is characteristic for the seismic mid-lithosphere discontinuity, a zone of low seismic velocities that is widespread in the continental lithospheric mantle, and is found intermittently beneath all continents at a depth of 80 to 100 km. The mid-lithosphere discontinuity has been suggested to be related to the occurrence of hydrous assemblages (*32*, *33*), which is consistent with the formation of mica in our experiments.

Kimberlite magmas are generally considered to originate from partial melting of a carbonated peridotite source (*34*, *35*). The occurrence of Na-rich mineral and fluid inclusions in olivine phenocrysts in kimberlites (*36*–*38*) is consistent with the presence of primary Na-Ca carbonatite melts. The loss of sodium is thought to occur after emplacement by rapid weathering of the kimberlite matrix (*18*, *39*). The Udachnaya-East kimberlite is a very fresh chlorine-rich kimberlite that has been used to propose that Cl-rich carbonatite may be a common protokimberlitic composition (*18*, *39*). Our experimental observation of Na-K chlorides coexisting with carbonate in the reaction zone between sedimentary rock and peridotite may thus be directly relevant for the source of some kimberlites. Melting experiments on chloride-rich Udachnaya-East kimberlites (*40*) at 4.5 to 6.5 GPa/1000° to 1100°C within the carbonated peridotite stability field have produced melts close to the composition of diamond microinclusions of high-Mg carbonatitic composition (Fig. 4) (*19*). Hence, our experiments provide evidence that the reaction between sediment-derived melts and mantle peridotite at >120 km can produce the same fluids that are trapped in diamonds. These fluids precipitate chlorides as a direct result of migrating into the strongly reduced environment of the lower cratonic mantle, producing sources that may later melt to form exotic chloride-bearing alkaline kimberlites such as those found at Udachnaya-East.

MATERIALS AND METHODS

The sediment sample used as a starting material in the experiments was acquired from the International Ocean Discovery Project (ODP 161-976 B 18 X3 105-106.5) and is a carbonate-bearing (<10%) siliciclastic marine sediment (table S1) similar to global subducting sediment composition (*41*) but with higher contents of carbonate. For the depleted peridotite, we used a clinopyroxene-bearing dunite (sample ZD11–53) containing olivine (>97%), spinel (~2%), and clinopyroxene (<1%) from the Zedang ophiolite (south Tibet, China), which occurs as a lens-shaped body within harzburgite (table S2). The dunite was chosen because it represents the most depleted end-member of peridotites that are present within the lithospheric mantle. Furthermore, all metasomatic phases that grow during the experiment are easy to recognize and cannot be confused with phases that are already present in less depleted peridotite. Both samples were ground to powders in an agate mortar. Experiments were carried out using a piston cylinder apparatus at the University of Mainz at 3 GPa and a belt apparatus at Goethe Universität Frankfurt at 4 to 6 GPa. Sediment and peridotite powders were placed as separate layers in an inner carbon capsule, which controls fO_2 via the C + CO equilibrium. The inner carbon capsule was sealed in an outer platinum capsule. For the piston cylinder experiments, the experimental assembly consisted of a pressure cell made of Al_2O_3 spacers, a graphite furnace, B-type thermocouple, and a CaF_2 spacer outside the capsule. For belt apparatus experiments, most of the materials were similar to piston-cylinder experiments, but the spacer and capsule holder consisted of natural polycrystalline calcium fluoride. All cell assemblies were first pressurized and subsequently heated at a rate of 50°C/min. Thermobaric conditions were kept constant for 2 to 14 days. At the end of each experiment, charges were quenched by switching off the heating. Quench times to temperatures below 500°C were approximately 6 s for the piston-cylinder runs and 8 s for the belt runs. Major element compositions of phases in experimental run products were acquired using a JEOL JXA 8200 SuperProbe electron-probe microanalyzer equipped with five wavelength dispersive spectrometers at the University of Mainz, Germany. Micas, silicates, and glasses were analyzed with an accelerating voltage of 15 kV and a beam current of 12 nA. Peak counting times were 20 to 30 s for melts and silicate minerals. The beam diameter was set to 2 μm. Element maps and semiquantitative energy-dispersive x-ray analysis were performed using a nanoScience Instruments Phenom XL benchtop electron microscope. Three aliquots of the sediment were analyzed for H, C, and N in an automated vario EL cube elemental analyzer (Elementar, Langenselbold, Germany) using the method described by Le Huong *et al.* (*42*). Analyses of SDO-1 (U.S. Geological Survey reference material—shale) yielded H = 1.57 ± 0.14 wt %, C = 9.11 ± 0.01 wt %, and N = 0.36 ± 0.01 wt %, within error of the GeoReM (http://georem.mpch-mainz.gwdg.de/) (*43*) compiled values for H and C (H = 1.34 wt %; C = 9.95 wt %).

SUPPLEMENTARY MATERIALS

Supplementary material for this article is available at http://advances.sciencemag.org/cgi/content/full/5/5/eaau2620/DC1

Fig. S1. Modal proportions of phases in the reaction experiments and the melting experiment.
Fig. S2. K/Na and Cl/F in mica, melt, fluid, and solid halide phases (chlorides + fluorides).
Fig. S3. Chloride map of 5 GPa/1000°C experiment.
Fig. S4. Backscattered electron image of the 6 GPa/1100°C experiment showing an unpolished capsule half.
Fig. S5. Composition of silicate phases in reaction experiments.
Table S1. Phase relations of experiments.
Table S2. Starting materials.
Table S3. Reaction experiment (3 GPa/800°C).
Table S4. Reaction experiment (3 GPa/850°C).
Table S5. Reaction experiment (3 GPa/900°C).
Table S6. Reaction experiment (3 GPa/1000°C).
Table S7. Reaction experiment (4 GPa/900°C).
Table S8. Sediment melting (4 GPa/1000°C).
Table S9. Reaction experiment (4 GPa/1000°C).
Table S10. Reaction experiment (4 GPa/1100°C).
Table S11. Reaction experiment (5 GPa/1000°C).
Table S12. Reaction experiment (6 GPa/1100°C).
Table S13. Mass balance of 3 GPa/800°C reaction experiment.
Table S14. Mass balance of 3 GPa/850°C reaction experiment.
Table S15. Mass balance of 3 GPa/1000°C reaction experiment.
Table S16. Mass balance of 4 GPa/1100°C reaction experiment.
Table S17. Mass balance of 4 GPa/1000°C sediment melting experiment.
Table S18. Mass balance of 5 GPa/1000°C reaction experiment.
Reference (*45*)

REFERENCES AND NOTES

1. W. L. Griffin, S. Y. O'Reilly, J. C. Afonso, G. C. Begg, The composition and evolution of lithospheric mantle: A re-evaluation and its tectonic implications. *J. Petrol.* **50**, 1185–1204 (2008).
2. Y. Weiss, J. McNeill, D. G. Pearson, G. M. Nowell, C. J. Ottley, Highly saline fluids from a subducting slab as the source for fluid-rich diamonds. *Nature* **524**, 339–342 (2015).

3. S. F. Foley, T. P. Fischer, An essential role for continental rifts and lithosphere in the deep carbon cycle. *Nat. Geosci.* **10**, 897–902 (2017).
4. B. M. Jablon, O. Navon, Most diamonds were created equal. *Earth Planet. Sci. Lett.* **443**, 41–47 (2016).
5. Y. N. Pal'yanov, A. G. Sokol, Y. M. Borzdov, A. F. Khokhryakov, N. V. Sobolev, Diamond formation from mantle carbonate fluids. *Nature* **400**, 417–418 (1999).
6. C. S. Eldridge, W. Compston, I. S. Williams, J. W. Harris, J. W. Bristow, Isotope evidence for the involvement of recycled sediments in diamond formation. *Nature* **353**, 649–653 (1991).
7. E. L. Tomlinson, A. P. Jones, J. W. Harris, Co-existing fluid and silicate inclusions in mantle diamond. *Earth Planet. Sci. Lett.* **250**, 581–595 (2006).
8. E. S. Izraeli, J. W. Harris, O. Navon, Brine inclusions in diamonds. *Earth Planet. Sci. Lett.* **187**, 323–332 (2001).
9. Y. Weiss, R. Kessel, W. L. Griffin, I. Kiflawi, O. Klein-BenDavid, D. R. Bell, J. W. Harris, O. Navon, A new model for the evolution of diamond-forming fluids: Evidence from microinclusion-bearing diamonds from Kankan, Guinea. *Lithos* **112**, 660–674 (2009).
10. S. E. Haggerty, A diamond trilogy. *Science* **285**, 851–860 (1999).
11. B. A. Kjarsgaard, D. G. Pearson, S. Tappe, G. M. Nowell, D. P. Dowall, Geochemistry of hypabyssal kimberlites from Lac de Gras, Canada: Comparisons to a global database and applications to the parent magma problem. *Lithos* **112**, 236–248 (2009).
12. R. H. Mitchell, *Kimberlites, Mineralogy, Geochemistry, and Petrology* (Springer Science & Business Media, 2013).
13. A. E. Ringwood, S. E. Kesson, W. Hibberson, N. Ware, Origin of kimberlites and related magmas. *Earth Planet. Sci. Lett.* **113**, 521–538 (1992).
14. M. Harris, A. Le Roex, C. Class, Geochemistry of the Uintjiesberg kimberlite, South Africa: Petrogenesis of an off-craton, group I, kimberlite. *Lithos* **74**, 149–165 (2004).
15. S. F. Foley, G. M. Yaxley, A. Rosenthal, S. Buhre, E. S. Kiseeva, R. P. Rapp, D. E. Jacob, The composition of near-solidus melts of peridotite in the presence of CO_2 and H_2O between 40 and 60 kbar. *Lithos* **112**, 274–283 (2009).
16. M. G. Kopylova, S. I. Kostrovitsky, K. N. Egorov, Salts in southern Yakutian kimberlites and the problem of primary alkali kimberlite melts. *Earth-Sci. Rev.* **119**, 1–16 (2013).
17. N. Stamm, M. W. Schmidt, Asthenospheric kimberlites: Volatile contents and bulk compositions at 7 GPa. *Earth Planet. Sci. Lett.* **474**, 309–321 (2017).
18. V. S. Kamenetsky, A. V. Golovin, R. Maas, A. Giuliani, M. B. Kamenetsky, Y. Weiss, Towards a new model for kimberlite petrogenesis: Evidence from unaltered kimberlites and mantle minerals. *Earth-Sci. Rev.* **139**, 145–167 (2014).
19. Y. Weiss, W. L. Griffin, D. R. Bell, O. Navon, High-Mg carbonatitic melts in diamonds, kimberlites and the sub-continental lithosphere. *Earth Planet. Sci. Lett.* **309**, 337–347 (2011).
20. D. Jacob, E. Jagoutz, D. Lowry, D. Mattey, G. Kudrjavtseva, Diamondiferous eclogites from Siberia: Remnants of Archean oceanic crust. *Geochim. Cosmochim. Acta* **58**, 5191–5207 (1994).
21. C. Spandler, J. Hermann, R. Arculus, J. Mavrogenes, Redistribution of trace elements during prograde metamorphism from lawsonite blueschist to eclogite facies; implications for deep subduction-zone processes. *Contrib. Mineral. Petrol.* **146**, 205–222 (2003).
22. J. Hermann, C. J. Spandler, Sediment melts at sub-arc depths: An experimental study. *J. Petrol.* **49**, 717–740 (2007).
23. Y. Wang, D. Prelević, S. Buhre, S. F. Foley, Constraints on the sources of post-collisional K-rich magmatism: The roles of continental clastic sediments and terrigenous blueschists. *Chem. Geol.* **455**, 192–207 (2017).
24. E. M. Syracuse, P. E. van Keken, G. A. Abers, The global range of subduction zone thermal models. *Phys. Earth Planet. Inter.* **183**, 73–90 (2010).
25. G. Chiodini, L. Marini, Hydrothermal gas equilibria: The H_2O-H_2-CO_2-CO-CH_4 system. *Geochim. Cosmochim. Acta* **62**, 2673–2687 (1998).
26. S. Jakobsson, N. Oskarsson, The system CO in equilibrium with graphite at high pressure and temperature: An experimental study. *Geochim. Cosmochim. Acta* **58**, 9–17 (1994).
27. A. Wang, J. D. Pasteris, H. O. A. Meyer, M. L. Dele-Duboi, Magnesite-bearing inclusion assemblage in natural diamond. *Earth Planet. Sci. Lett.* **141**, 293–306 (1996).
28. H. P. Scott, R. J. Hemley, H.-k. Mao, D. R. Herschbach, L. E. Fried, W. M. Howard, S. Bastea, Generation of methane in the Earth's mantle: In situ high pressure–temperature measurements of carbonate reduction. *Proc. Natl. Acad. Sci. U.S.A.* **101**, 14023–14026 (2004).
29. N. S. Martirosyan, T. Yoshino, A. Shatskiy, A. D. Chanyshev, K. D. Litasov, The $CaCO_3$–Fe interaction: Kinetic approach for carbonate subduction to the deep Earth's mantle. *Phys. Earth Planet. Inter.* **259**, 1–9 (2016).
30. Y. Weiss, O. Navon, S. L. Goldstein, J. W. Harris, Inclusions in diamonds constrain thermo-chemical conditions during Mesozoic metasomatism of the Kaapvaal cratonic mantle. *Earth Planet. Sci. Lett.* **491**, 134–147 (2018).
31. D. A. Ionov, L. S. Doucet, I. V. Ashchepkov, Composition of the lithospheric mantle in the Siberian craton: New constraints from fresh peridotites in the Udachnaya-East kimberlite. *J. Petrol.* **51**, 2177–2210 (2010).
32. K. Selway, H. Ford, P. Kelemen, The seismic mid-lithosphere discontinuity. *Earth Planet. Sci. Lett.* **414**, 45–57 (2015).
33. S. M. Hansen, K. Dueker, B. Schmandt, Thermal classification of lithospheric discontinuities beneath USArray. *Earth Planet. Sci. Lett.* **431**, 36–47 (2015).
34. R. H. Mitchell, Experimental studies at 5–12 GPa of the Ondermatjie hypabyssal kimberlite. *Lithos* **76**, 551–564 (2004).
35. A. G. Sokol, I. N. Kupriyanov, Y. N. Palyanov, A. N. Kruk, N. V. Sobolev, Melting experiments on the Udachnaya kimberlite at 6.3–7.5 GPa: Implications for the role of H_2O in magma generation and formation of hydrous olivine. *Geochim. Cosmochim. Acta* **101**, 133–155 (2013).
36. T. P. Mernagh, V. S. Kamenetsky, M. B. Kamenetsky, A Raman microprobe study of melt inclusions in kimberlites from Siberia, Canada, SW Greenland and South Africa. *Spectrochim. Acta Part A* **80**, 82–87 (2011).
37. A. Giuliani, V. S. Kamenetsky, D. Phillips, M. A. Kendrick, B. A. Wyatt, K. Goemann, Nature of alkali-carbonate fluids in the sub-continental lithospheric mantle. *Geology* **40**, 967–970 (2012).
38. A. Giuliani, V. S. Kamenetsky, M. A. Kendrick, D. Phillips, B. A. Wyatt, R. Maas, Oxide, sulphide and carbonate minerals in a mantle polymict breccia: Metasomatism by proto-kimberlite magmas, and relationship to the kimberlite megacrystic suite. *Chem. Geol.* **353**, 4–18 (2013).
39. V. S. Kamenetsky, M. B. Kamenetsky, A. V. Golovin, V. V. Sharygin, R. Maas, Ultrafresh salty kimberlite of the Udachnaya–East pipe (Yakutia, Russia): A petrological oddity or fortuitous discovery? *Lithos* **152**, 173–186 (2012).
40. I. S. Sharygin, K. D. Litasov, A. Shatskiy, A. V. Golovin, E. Ohtani, N. P. Pokhilenko, Melting phase relations of the Udachnaya-East group-I kimberlite at 3.0–6.5 GPa: Experimental evidence for alkali-carbonatite composition of primary kimberlite melts and implications for mantle plumes. *Gondwana Res.* **28**, 1391–1414 (2015).
41. T. Plank, C. H. Langmuir, The chemical composition of subducting sediment and its consequences for the crust and mantle. *Chem. Geol.* **145**, 325–394 (1998).
42. L. T.-T. Le Huong, L. M. Otter, M. W. Förster, C. A. Hauzenberger, K. Krenn, O. Alard, D. S. Macholdt, U. Weis, B. Stoll, K. P. Jochum, Femtosecond laser ablation-ICP-mass spectrometry and CHNS elemental analyzer reveal trace element characteristics of danburite from Mexico, Tanzania, and Vietnam. *Fortschr. Mineral.* **8**, 234 (2018).
43. K. P. Jochum, U. Nohl, K. Herwig, E. Lammel, B. Stoll, A. W. Hofmann, GeoReM: A new geochemical database for reference materials and isotopic standards. *Geostand. Geoanal. Res.* **29**, 333–338 (2005).
44. J. K. Russell, L. A. Porritt, Y. Lavallée, D. B. Dingwell, Kimberlite ascent by assimilation-fuelled buoyancy. *Nature* **481**, 352–356 (2012).
45. A. D. Pelton, A. Gabriel, J. Sangster, Liquidus measurements and coupled thermodynamic–phase-diagram analysis of the NaCl–KCl system. *J. Chem. Soc. Faraday Trans. 1* **81**, 1167–1172 (1985).

Acknowledgments: We acknowledge the Macquarie University Faculty of Science and Engineering Microscope Facility (MQFoSE MF) for access to its instrumentation and support from its staff. We thank T. Kautz (Goethe Universität Frankfurt) for assistance with belt apparatus experiments. We acknowledge D. Jacob and B. Griffin for proofreading this manuscript. We also thank O. Navon and Y. Weiss for reviewing and improving the final version of the paper. This is contribution 1331 from the ARC Centre of Excellence for Core to Crust Fluid Systems (www.ccfs.mq.edu.au) and 1305 in the GEMOC Key Centre (www.gemoc.mq.edu.au). **Funding:** This work is part of the PhD thesis of M.W.F., supported by an Australian Government International Postgraduate Research Scholarship (IPRS), Macquarie Postgraduate Research Fund (PGRF), and the ARC Centre of Excellence for Core to Crust Fluid Systems (CCFS). H.R.M. acknowledges support from the Wilhelm und Else Heraeus Stiftung, and S.F.F. acknowledges ARC grant FL180100134. The International Ocean Discovery Project (IODP) provided the Mediterranean marine sediment. **Author contributions:** S.F.F., M.W.F., and H.R.M. designed the study and wrote the manuscript. M.W.F. and S.B. carried out the experiments. S.B. and O.A. performed analytical measurements. All authors carefully edited the final version of the manuscript. **Competing interests:** The authors declare that they have no competing interests. **Data and materials availability:** All data needed to evaluate the conclusions in the paper are present in the paper and/or the Supplementary Materials. Additional data related to this paper may be requested from the authors.

Submitted 23 May 2018
Accepted 17 April 2019
Published 29 May 2019
10.1126/sciadv.aau2620

Citation: M. W. Förster, S. F. Foley, H. R. Marschall, O. Alard, S. Buhre, Melting of sediments in the deep mantle produces saline fluid inclusions in diamonds. *Sci. Adv.* **5**, eaau2620 (2019).

Science Advances

Melting of sediments in the deep mantle produces saline fluid inclusions in diamonds

Michael W. Förster, Stephen F. Foley, Horst R. Marschall, Olivier Alard and Stephan Buhre

Sci Adv **5** (5), eaau2620.
DOI: 10.1126/sciadv.aau2620